Journal of the Serbian Chemical Society
JSCS@tmf.bg.ac.rs • www.shd.org.rs/JSCS

J. Serb. Chem. Soc. 90 (10) 1175–1187 (2025)
JSCS–5447

Original scientific paper
Published 26 October, 2025

N-Phenyl-3-sulfamoyl-benzamide derivatives as anti-Hepatitis B virus agent candidates. Integrated computational studies

AICHA LAOUD[1], ABDERAHMANE BELAFRIEKH[2]* and MARWA ALAQARBEH[3]

[1]Chemical Engineering Department, Faculty of Chemical Engineering, University of Salah Boubnider Constantine 3, Constantine, 25000, Algeria, [2]Laboratory of LCPMM, Chemistry Department, Faculty of Sciences, University of Blida1, P.O. Box 270 Blida, 09000, Algeria and [3]Basic Science Department, Prince Al Hussein Bin Abdullah II Academy for Civil Protection, Al-Balqa Applied University, Al-Salt, Jordan

(Received 30 April, revised 19 June, accepted 4 August 2025)

Abstract: This study used a combined approach of atom-based 3D-QSAR modeling and molecular docking to investigate 44 *N*-phenyl-3-sulfamoyl-benzamide derivatives as potential inhibitors of the hepatitis B virus (HBV). The developed QSAR model demonstrated strong statistical robustness, with a good correlation coefficient for the training set (R^2 = 0.94), a cross-validated coefficient (Q^2cv = = 0.65), and a correlation coefficient for the test set (R^2 = 0.85) using three PLS--components. Contour maps explained the modified areas within the compounds, clarifying hydrogen bond donors, hydrophobic interactions and electrostatic effects. The docking studies supported the findings of the 3D-QSAR model and explained the molecule's interactions with the receptors. Overall, the model and the docking analysis provide valuable insights into designing molecules with enhanced activity against the hepatitis B virus.

Keywords: molecular docking; HBV; 3D-QSAR; coefficient.

INTRODUCTION

The Hepatitis B virus (HBV) is the etiological agent of Hepatitis B, a serious viral infection that represents a significant global public health concern.[1] This disease primarily affects the liver and has the potential to progress to chronic hepatitis, cirrhosis and hepatocellular carcinoma.[2] HBV is easily transmitted through blood by sexual contact and from mother to child during pregnancy, underscoring the critical importance of implementing robust prevention strategies.[3] Recent advancements in vaccines and antiviral therapies have substantially reduced the transmission of HBV and the mortality associated with it. Despite these positive developments, significant challenges persist, particularly in resource-constrained

* Corresponding author. E-mail: a.belafriekh@gmail.com
https://doi.org/10.2298/JSC250430060L

environments where access to medical care and vaccinations is limited.[4] Furthermore, recent medicinal alternatives cannot eradicate covalently closed circular DNA (cccDNA), which serves as a reservoir for persistent viral infection, effectively complicating efforts to annihilate the disease.[5]

Current antiviral medications are effective in inhibiting the replication of viruses; however, they are incapable of completely eradicating them. This study underscores the necessity for innovative therapeutic strategies.[6,7] The primary objective of this research is to enhance our understanding of the mechanisms by which the Hepatitis B virus (HBV) operates and to develop novel antiviral agents that can effectively prevent viral transmission, circumvent drug resistance and progress toward a definitive cure. The current study aims to predict the anti-Hepatitis B activity of forty-four *N*-phenyl-3-sulfamoyl-benzamide derivatives[8] using an atom-based 3D-QSAR model and molecular docking to understand binding interactions with key HBV proteins. In this research, several computational methods, such as molecular docking and quantitative structure–activity relationship (QSAR) modeling, were used in identifying potential HBV inhibitors by analyzing the relationship between molecular structures and their antiviral effectiveness.[9,10]

EXPERIMENTAL

Dataset

A series of forty-four *N*-phenyl-3-sulfamoyl-benzamide derivatives (Table S-I of the Supplementary material to this paper) were identified from the literature as inhibitors of the Hepatitis B virus (HBV).[8] The half-maximal effective concentration (EC_{50}) values were transformed into their corresponding pEC_{50} values (pEC_{50} = –log ($EC_{50}\times10^{-6}$)) to reduce data skewness and facilitate analysis. The dataset was subsequently divided into two subsets to develop a 3D-QSAR model: randomly, 33 compounds were selected to be the training set for building the model. The other 11 compounds were used as the test set to see how well the proposed model could predict the future.[11]

Ligand preparation

ChemDraw Ultra drew all the 2D structures in the dataset and then imported them into the Maestro interface to generate 3D structures.[12] The generated 3D structures were prepared using the LigPrep module with an OPLS-2005 force field.[13] To ensure comprehensive representation, multiple tautomers and potential ionization states were generated and considered within a pH range of 7±2, with all other parameters kept at their default settings.[14]

Molecular docking

The crystal structure of the Hepatitis B virus core protein (PDB ID: 5T2P, resolution: 1.69 Å) was retrieved from the Protein Data Bank (https://www.rcsb.org/structure). Protein preparation was performed using the Protein Preparation Wizard module in Maestro.[15] During this process, all water molecules were removed, and hydrogen atoms were added. The protein structure was energy-minimized using the OPLS-2005 force field, with a root-mean-square deviation (*RMSD*) threshold of 0.30 Å,[16] A receptor grid was generated using the Co-crystallized ligand (K89) as the centroid, with de coordinates X= -0.96 Å, Y= 40.16 Å, and Z= -6.88 Å.[17] Molecular docking techniques help scientists to predict binding modes and interaction

profiles with the virus. The Glide extra-precision (XP) module was then used for docking studies to check ligand docking scores and binding affinities at the target protein's active site.[18,19]

Atom-based 3D-QSAR model generation

A 3D-QSAR model was developed using the atom-based QSAR feature in the Phase module to predict the anti-Hepatitis B inhibitory activity of selected compounds.[20] The dataset was initially divided into training and test sets using a random selection method, with a ratio of 75:25.[21] The model development was carried out using partial least squares (PLS) regression with a grid spacing of 1 Å.[22] The primary criterion for selecting the optimal model was statistical robustness, further visualized through contour maps. The performance and stability of the model were evaluated using metrics such as *SD*, R^2, R^2cv, stability, *F*, *P*, *RMSE*, Q^2 and Pearson-*r*. Internal validation of the training set was performed using a leave-one-out (LOO) cross-validation method to calculate R^2 and R^2cv.[23,24] External validation with the test set confirmed the model's predictive accuracy, as assessed by Q^2 and other relevant parameters.[25] A scatter plots was created to depict the relationship between predicted and observed activity values for both the training and test sets. Finally, the QSAR model was applied to predict the biological activity of newly designed molecules.

ADMET prediction and activity predicted (pEC_{50})

The newly designed compounds were subjected to Atom-based 3D-QSAR to predict their biological activity (pEC_{50}) based on the generated 3D-QSAR model. Additionally, the QikProp module in Schrödinger was used to predict the absorption, distribution, metabolism and excretion (ADME) properties of these compounds. These predictions provided insights into the pharmacokinetic profiles of the compounds, which are critical for assessing their potential as drug candidates.[26,27]

RESULTS AND DISCUSSION

Molecular alignment

Molecular alignment at the structural level is important for ensuring the accuracy of a 3D-QSAR model and the trustworthiness of the resulting contour maps. Consequently, a flexible alignment approach was utilized to align all selected anti-hepatitis compounds in this study. We chose the most active compound **8** as the template and aligned the remaining compounds based on their shared substructure (Fig. 1).

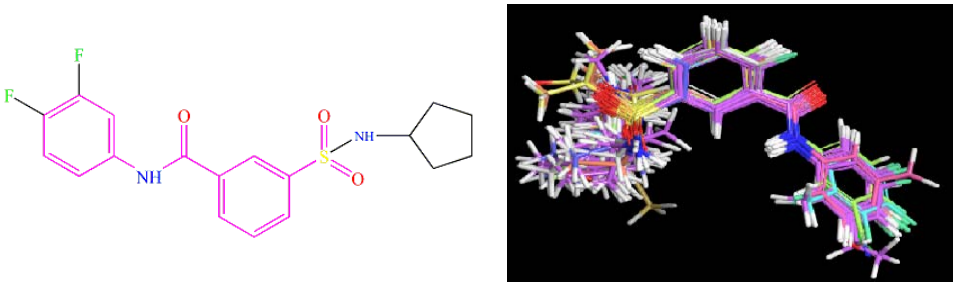

(a) (b)

Fig 1. a) Template used for molecular alignment of anti-Hepatitis B virus. b) Structural alignment of the dataset chosen for the QSAR model.

Molecular docking analysis of N*-phenyl-3-sulfamoyl-benzamide derivatives*

The binding affinity of the ligand Co-crystalline K89 (sulfamoylbenzamide, or SBA) was –44.40 kJ/mol. This ligand formed hydrogen bonds with the amino residues TRP102, LEU140 and THR128 (Fig. 2). The binding affinity for the *N*-phenyl-3-sulfamoyl-benzamide derivatives was similar to that of the ligand co--crystalline K89, ranging from –42.34 to –27.66 kJ/mol. These derivatives formed hydrogen bonds with the residues TRP102 and THR128 (refer to Fig. 2). These conserved hydrogen bonding interactions appear to be key determinants for the binding of this chemical series to the HBV core protein, suggesting a common binding mode and contributing significantly to the observed binding affinities. Beyond hydrogen bonding, a range of other important interactions contributed to the overall binding stability. Significant hydrophobic interactions were noted with the residues PHE23, TYR118, PRO25, ILE105, PRO138, TRP102, LEU101 and LEU140. These extensive hydrophobic contacts play a crucial role in anchoring the non-polar portions of the ligands within the hydrophobic pockets of the active site, thereby enhancing binding affinity through the hydrophobic effect. Furthermore, electrostatic interactions were observed, with a negatively charged interaction noted with ASP29 and a positively charged interaction with the residue ARG127.

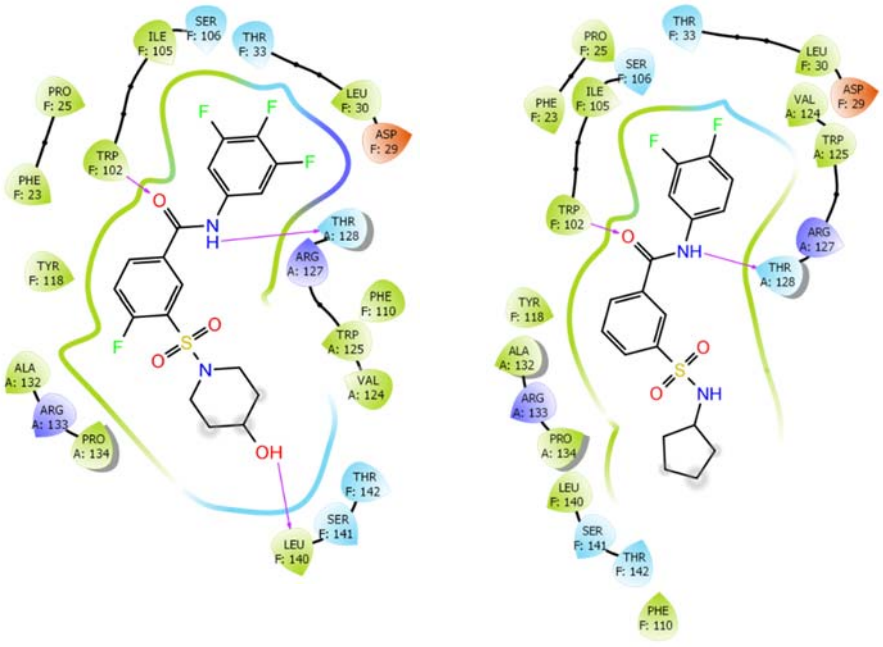

K89 Compound **8**

Fig. 2. 3D and 2D interaction between the Hepatitis B virus core protein (PDB ID: 5T2P) and the co-crystalline ligand (K89), as well as compound **8**.

These charged interactions contribute to the specificity and strength of binding, particularly when the ligand possesses complementary charges. Additionally, Polar interactions occurred with the amino acid residues SER106, SER121 and THR33, further supporting the overall ligand-receptor recognition.

Notably, compounds that exhibited higher predicted anti-HBV activity (higher pEC50 values from the QSAR model) consistently showed more favorable (lower) docking scores. It formed a greater number of these crucial stabilizing interactions (*e.g.*, hydrogen bonds with TRP102/THR128, extensive hydrophobic contacts and favorable electrostatic interactions). For instance, beyond compound **8** (illustrated in Fig. 2), compounds **5**, **7**, **38**, **39** and **42** demonstrated the most favorable binding affinities, aligning well with their predicted high biological activity.

In this study, a 3D-QSAR model was developed using the atom-based 3D--QSAR approach within the phase module. The model underwent internal validation with an R^2 value for the training set and external validation with a Q^2 value for the test set. Table I summarizes the statistical parameters. The results revealed a strong correlation between the predicted and actual activity values, as shown in Table II, demonstrating the model's predictive capability. The QSAR model exhibited strong predictive performance, with key values of $R^2 = 0.94$, R^2cv = 0.61, and $Q^2 = 0.85$, indicating its reliability. Furthermore, the low standard deviation (*SD*) of 0.17 and *RMSE* of 0.18 underscored the high quality of the dataset for QSAR analysis. Fig. 3 illustrates the correlation between the training and test sets' actual and predicted pEC_{50} values. These findings pave the way for further research into optimizing compound design and enhancing drug efficacy in future studies.

TABLE I. PLS Statistics parameters of the 3D-QSAR model

PLS statistics	3D-QSAR model	Threshold
PLS: partial least square	3	*N* training set: 5
SD: standard deviation	0.17	Smaller value
R^2: Regression coefficient	0.94	>0.6
R^2_{cv}: cross-validated correlation coefficient	0.61	>0.5
Stability	0.755	Maximal value of 1
F: ratio of the model variance	151.8	High value
P: significance level of variance ratio	7.94e–18	Smaller value
RMSE: root-mean-square error	0.18	Smaller value
Q^2: Correlation coefficient for the test set	0.85	>0.6
Pearson-*r*: correlation between the predicted and observed activity	0.85	–
Contribution, %		
H-bond donor	7	–
Hydrophobic	68	–
Positive ionic	2.9	–
Electrostatic	17.8	–
Other	4.3	–

3D-QSAR study

Four contributions were applied in the construction of the model: H-bond donor, hydrophobic, positive and electrostatic. Table I shows that the hydrophobic (68 %) and electrostatic (17.8 %) groups contributed most to anti-Hepatitis B activity.

TABLE II. Actual (pEC_{50}) and predicted (pEC_{50pred}) values along with the residual of the dataset

N	EC_{50}	pEC_{50}	pEC_{50Pred}	Residual	*N*	EC_{50}	pEC_{50}	pEC_{50Pred}	Residual
Training Set					32	2.22	5.65	5.72	0.07
2	0.78	6.11	6.26	0.15	33	3.63	5.44	5.46	0.02
4	0.60	6.22	6.12	–0.10	34	0.38	6.08	6.29	0.21
5	0.36	6.44	6.40	–0.04	36	2.33	5.63	5.91	0.28
7	0.27	6.57	6.36	–0.21	37	0.07	7.16	7.10	–0.06
8	0.038	7.41	6.99	–0.42	38	0.31	6.51	6.50	0.01
11	1.99	5.70	5.90	0.20	39	0.21	6.68	6.80	0.12
13	26.5	4.58	4.40	–0.18	40	1.40	5.85	5.88	0.03
14	7.10	5.15	5.07	–0.08	41	0.32	6.50	6.28	–0.21
15	8.49	5.07	5.06	–0.01	42	2.74	6.92	6.89	–0.03
16	4.53	5.34	5.29	–0.05	44	3.06	5.51	5.65	0.14
18	0.75	6.13	6.23	0.10	Test set				
20	0.34	6.47	6.29	–0.18	1	2.60	5.86	5.63	0.05
22	2.10	6.08	6.06	–0.02	3	0.66	6.18	6.38	0.20
23	0.96	5.68	5.87	0.20	6	4.18	5.38	5.25	–0.13
24	1.18	6.02	5.82	–0.20	9	0.28	6.55	6.25	–0.30
25	0.54	5.93	6.04	0.12	10	0.10	7.00	6.93	0.07
26	6.77	6.27	6.40	0.13	12	4.50	5.35	5.13	–0.22
27	5.30	5.17	5.13	–0.04	17	0.74	6.13	5.99	–0.14
28	0.93	5.27	5.16	–0.12	19	0.75	6.13	6.16	0.03
29	0.12	6.03	6.23	0.20	21	1.21	5.91	5.93	0.02
30	2.10	6.92	6.77	–0.15	35	0.81	6.09	6.16	0.07
31	0.29	6.54	6.67	0.13	43	3.06	5.56	5.95	0.38

Contour plots of the 3D-QSAR model

Contour plots from a quantitative structure–activity relationship (3D-QSAR) model are valuable tools for gaining a deeper understanding of how the molecular properties of compounds influence their biological activity.[28,29] It is particularly important in the context of 3D-QSAR analysis. These plots can show regions where specific interactions (such as hydrogen bond donor, electrostatic or hydrophobic interactions) are favorable or unfavorable for biological activity.[30] The results contribute to the development of new selective agents and inhibitors for the hepatitis B virus. In Fig. 4, the contour plots utilize compound **8** as a reference to illustrate how hydrogen bond donor, electrostatic, and hydrophobic interactions influence the compound's effectiveness in combating the virus.

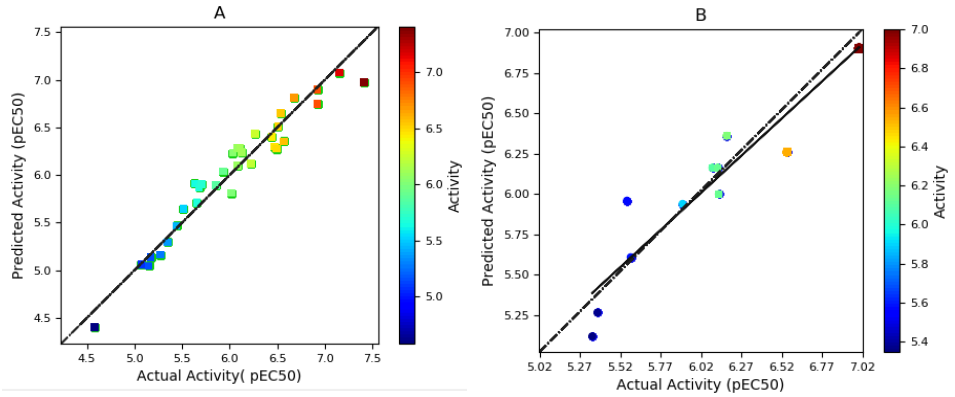

Fig. 3. Graph of predicted *vs*. actual pEC_{50} values for the training set (A) and test set (B).

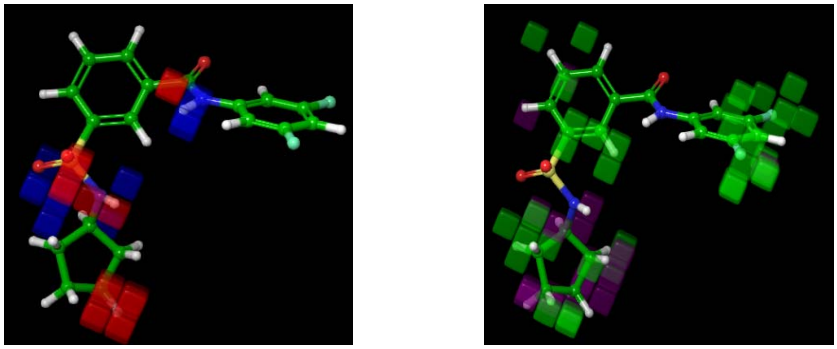

a) H-bond donor effect: 7 % b) Hydrophobic effect: 68 %

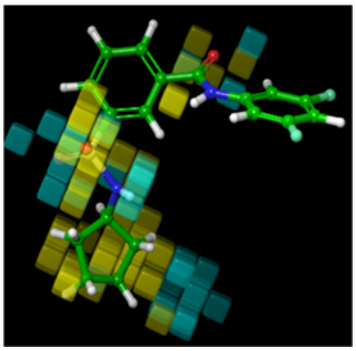

c) Electrostatic effect: 17.8 %

Fig. 4. Visualization of atom-based 3D-QSAR contour maps for the most active compound **8**.

In the hydrogen bond donor effect (Fig. 4a), the blue cube suggests that the hydrogen bond donor groups (such as –NH or –OH groups) can improve biological activity, while the red cube suggests that some of these groups can be detrimental to biological activity. The blue cubes are located near the amid group (–CO–NH–)

and sulfonamide (–NH–SO_2–) group compounds. The location suggests that these groups can interact favorably with the biological target *via* hydrogen bonds, thereby increasing the compound's activity.

In the hydrophobic effect (Fig. 4b), the green cubes indicate regions where hydrophobic interactions can enhance biological activity. Green cubes are near the compound's phenyl and cyclopentane groups. These hydrophobic interactions may promote the compound's adhesion to the biological target or help stabilize the active conformation. Purple cubes indicate regions where hydrophobic interactions are unfavorable and impair biological activity. Also, the green cubes seen near the fluorinated groups on the phenyl group show that these hydrophobic interactions are good for activity.

In the electrostatic effect (Fig. 4c), the yellow cubes indicate that electrostatic groups enhance biological activity. Electrostatic groups withdraw electrons, making the compound more reactive and improving its interaction with the biological target. The presence of yellow cubes near the sulfonamide group and the amid group suggests that these groups promote beneficial interactions for activity. In contrast, the cyan cubes show regions where electrostatic groups can impair biological activity.

Design of new inhibitors of Hepatitis B

The molecular docking analysis of the new compounds (Fig. S-1 of the Supplementary material) revealed a π–π interaction with the amino acid PHE110. While a hydrogen bond acceptor interaction was observed at residue THR196, hydrogen bond donor interactions were noted at residues THR33, THR128 and LEU140. The binding affinity for the newly designed compounds (ranging from –44.14 to –39.24 kJ mol^{-1}) was analogous to that of the *N*-phenyl-3-sulfamoyl--benzamide derivatives (range: –42.34 to –26.02 kJ mol^{-1}), suggesting that the newly designed compounds exhibited a higher binding affinity for the inhibition of Hepatitis B. The 2D ligand interaction diagram for the newly designed compounds is shown in Fig S-1. Additionally, the docking results of the newly designed compounds and their predicted pEC_{50} values are detailed in Table III.

TABLE III. Molecular docking results and predicted pEC_{50} values of the newly designed compounds

Design	XP-Gscore (kJ/mol^{-1})	E-model (kJ/mol^{-1})	Key interacting residues	pEC_{50} Predict
D1	–44.14	–388.40	LEU140, PHE110, THR128, TRP102, THR38	5.46
D2	–42.84	–364.30	LEU140, PHE110, THR128, TRP102, THR38	5.60
D3	–42.47	–369.66	LEU140, PHE110, THR128, TRP102, THR38	5.56
D4	–42.09	–374.22	LEU140, PHE110, THR128, TRP102	5.81

TABLE III. Continued

Design	XP-Gscore (kJ/mol^{-1})	E-model (kJ/mol^{-1})	Key interacting residues	pEC_{50} Predict
D5	–42.05	–335.31	LEU140, PHE110, THR128, TRP102	5.62
D6	–41.09	–389.07	LEU140, PHE110, THR128, TRP102	5.82
D7	–40.71	–378.69	LEU140, PHE110, THR128, TRP102	6.17
D8	–39.24	–355.56	LEU140, PHE110, VAL124, TRP102	5.87
K89	–44.60	–417.06	LEU140, THR128, TRP102	/
08	–42.34	–303.13	THR128, TRP102	/

ADME-Tox of the newly designed molecules

The evaluated ADME properties indicate that the newly designed molecules exhibit favorable pharmacokinetic characteristics (Tables IV and V).

TABLE IV. Results of drug-likeness parameters; *MW*: molecular weight; *HBD*: hydrogen bond donor; *HBA*: hydrogen bond acceptor; *PSA*: polar surface area

Design	*MW*	*HBA*	*HBD*	*PSA*	Rule of five	Rule of three
D1	377.43	3.50	8.00	110.85	0	0
D2	378.42	3.00	7.75	107.18	0	0
D3	378.42	3.00	7.75	106.63	0	0
D4	396.41	3.00	7.75	106.49	0	0
D5	378.42	3.00	7.75	107.33	0	0
D6	378.42	3.00	7.75	105.53	0	0
D7	396.41	3.00	7.75	105.52	0	0
D8	377.43	3.50	8.00	108.76	0	0
Rule	>500	0 to 6	2 to 20	140	N. Viol _ 1	N. Viol _ 1

All molecules show high human oral absorption (*HOA* = 3) and an acceptable percentage of oral absorption (P*HOA*, 75–83 %). The permeability across Caco-2 and MDCK cell lines varies, with some molecules, such as D6 and D7, demonstrating high permeability. This suggests they could be beneficial for transport across the intestinal and blood–brain barriers. Additionally, the *SASA* values fall within the optimal range (300–1000 Å^2), indicating that the molecular size and polarity are suitable. *QP*log*BB* indicates that some molecules have limited penetration into the brain, which can be advantageous if we want to avoid unwanted central nervous system (CNS) side effects. Predicted metabolic reactions (*metab*) fall within an acceptable range of 1 to 3, suggesting that the metabolic profiles are manageable. *QP*log*Khsa* values show standard binding to human serum albumin, which influences drug distribution. *QP*log*S* values demonstrate good solubility, supporting oral bioavailability. Additionally, *QP*log*Pw* and *QP*log*Po*/*w* values fall

within ideal ranges, indicating favorable lipophilicity and permeability. The *QP*log*HERG* value for most compounds is below –5.0, suggesting potential for *hERG* channel inhibition, which is a marker for cardiotoxicity risk. Additionally, no reactive functional groups (*RtvFG* = 0) were identified, which reduces the likelihood of off-target toxicity. These newly designed compounds show strong ADME profiles and exhibit drug-like potential.

TABLE V. Results of ADMET properties; *QP*log*Kp*: log *Kp* for skin permeability (< –2.5 for good permeability); *HOA*, human oral absorption (1 low, 3 high); *PHOA*, percent human oral absorption (80 % high, 25 % low); *QPPCaco*; predicted apparent Caco-2 cell permeability in nm s^{-1} (<25 poor,>500 great).QPPMDCK; Predicted apparent MDCK cell permeability in nm s^{-1} (<25 poor, >500 great); *SASA*, solvent-accessible surface area (300–1000 $Å^2$); *QP*log*BB*, predicted blood–brain partition coefficient (–1.5 to 1.5); *QP*log*Kha*, log *Khsa* serum protein binding (–1.5 to 1.5); *QP*logP_0*/w*, octanol–water partition coefficient (–2 to 6.5); *QP*log*Pw*, predicted water/gas partition coefficient (4 to 45); *metab*, prediction of metabolic activity (1 to 8); *QP*log*S*, predicted aqueous solubility, logarithm in mol dm^{-3} (–6.5 to 0.5); *Rotor*, number of rotatable bonds (0 to 15); *QP*log*HER*, for blocking HERG K^+ channel in terms of IC_{50} value (< –5.0); *RtvFG*, related to specific toxicity parameters (0 to 1, 0 indicating non-toxicity)

Parameter	D1	D2	D3	D4	D5	D6	D7	D8
*QP*log*Kp*	–3.66	–3.657	–3.322	–3.491	–3.497	–3.266	–3.386	–3.601
HOA	3	3	3	3	3	3	3	3
PHOA	76.97	79.17	80.74	81.75	79.73	81.86	83.06	77.59
QPPCaco	149.68	173.36	204.85	202.19	177.59	234.00	234.12	156.4
QPPMDCK	108.56	128.78	127.75	244.42	131.94	178.76	303.05	113.5
SASA	649.59	646.28	640.963	648.92	645.92	634.20	641.49	652.4
*QP*log*BB*	–1.64	–1.566	–1.488	–0.051	–0.059	–0.090	–0.058	–0.114
*QP*log*Kha*	–0.13	–0.083	–0.07	–0.051	–0.059	–0.090	–0.058	–0.114
*QP*logP_0*/w*	1.90	1.895	2.123	2.311	2.138	2.137	2.340	1.942
*QP*log*Pw*	15.879	14.864	14.913	14.65	14.87	14.75	14.55	15.91
metab	2	1	2	1	1	2	1	3
*QP*log*S*	–4.444	–4.462	–4.342	–4.804	–4.462	–4.462	–4.804	–4.324
Rotor	6	6	6	6	6	6	6	6
*QP*log*HER*	–5.710	–5.706	–5.562	–5.535	–5.645	–5.527	–5.403	–5.752
RtvFG	0	0	0	0	0	0	0	0

CONCLUSION

The current study successfully utilized a combination of atom-based 3D--QSAR modeling and molecular docking to investigate the efficacy of various *N*-phenyl-3-sulfamoyl benzamides as treatments for Hepatitis B and their mechanisms for inhibiting the virus. The developed 3D-QSAR model demonstrated a strong predictive capability with high correlation coefficients (R^2 = 0.94 for the training set, Q^2cv = 0.61, and Q^2 = 0.85 for the test set), reflecting a good agreement between experimental and theoretical results. The molecular docking studies were conducted to elucidate the binding interactions further and analyze how these molecules bind to the target HBV core protein. Additionally, ADMET predictions

suggested that the newly designed molecules possess favorable pharmacokinetic properties and drug-likeness, indicating their potential as promising candidates for further development. While these computational results provide strong theoretical support, it is important to acknowledge that in silico predictions have their limitations and require experimental validation. Future studies will focus on the synthesis and in *vitro* and in *vivo* testing of these promising compounds to experimentally confirm their anti-HBV activity and pharmacokinetic profiles. Overall, integrating QSAR modeling, docking studies, and ADMET profiling provides valuable insight into the rational design of novel antiviral agents targeting Hepatitis B.

SUPPLEMENTARY MATERIAL

Additional data and information are available electronically at the pages of journal website: https://www.shd-pub.org.rs/index.php/JSCS/article/view/13358, or from the corresponding author on request.

ИЗВОД

N-ФЕНИЛ-3-СУЛФАМОИЛ-БЕНЗАМИДНИ ДЕРИВАТИ КАО КАНДИДАТИ ЗА АНТИВИРУСНЕ АГЕНСЕ ПРОТИВ ХЕПАТИТИСА Б: ИНТЕГРИСАНЕ РАЧУНАРСКЕ СТУДИЈЕ

AICHA LAOUD[1], ABDERAHMANE BELAFRIEKH[2] и MARWA ALAQARBEH[3]

[1]Chemical Engineering Department, Faculty of Chemical Engineering, University of Salah Boubnider Constantine 3, Constantine, 25000, Algeria, [2]Laboratory of LCPMM, Chemistry Department, Faculty of Sciences, University of Blida1, P.O. Box 270 Blida, 09000, Algeria и [3]Basic Science Department, Prince Al Hussein Bin Abdullah II Academy for Civil Protection, Al-Balqa Applied University, Al-Salt, Jordan

У овом раду примењен је комбиновани приступ атомистички заснованог 3D-QSAR моделовања и молекулског докинга за испитивање 44 *N*-фенил-3-сулфамоил-бензамидних деривата као потенцијалних инхибитора вируса хепатитиса Б (HBV). Развијени QSAR модел показао је снажну статистичку поузданост, са високим коефицијентом корелације за тренинг сет (R^2 = 0,94), унакрсно валидираним коефицијентом (Q^2cv = 0,65), и коефицијентом корелације за тест сет (R^2 = 0,85), коришћењем три PLS-компоненте. Контурним мапама објашњени су модификовани региони једињења, прецизирајући доноре водоничних веза, хидрофобне интеракције и електростатичке ефекте. Докинг је потврдио резултате 3D-QSAR модела и објаснио интеракције молекула са рецепторима. Генерално, 3D-QSAR модел и анализа докинг резултата пружају важан увид у дизајн молекула са побољшаном активношћу против вируса хепатитиса Б.

(Примљено 30. априла, ревидирано 19. јуна, прихваћено 4. августа 2025)

REFERENCES

1. M. Kirstgen, S. F. Müller, K. Alessandra, A. Theresa, N. Goldmann, F. Lehmann, S. Alakurtti, J. Yli-kauhaluoma, K. Baringhaus, R. Krieg, D. Glebe, J. Geyer, *Viruses* **13** (2021) 1489 (https://doi.org/10.3390/v13081489)
2. C. Huang, Y. Jin, P. Fu, K. Hu, M. Wang, W. Zai, T. Hua, X. Song, J. Ye, Y. Zhang, G. Luo, H. Wang, J. Liu, J. Chen, X. Li,Z. Yuan, *Acta. Pharm. Sin., B* **14** (2024) 4914 (https://doi.org/10.1016/j.apsb.2024.07.019)

3. T. Ruengstra, A. Meeprasert, E. Rattanangkool, S. Deesiri, J. Srisa, U. Udomnilobol, W. Dunkoksung, N. Chuaypen, R. Kiatbumrung,P. Tangkijvanich, S. Vimolmangkang, K. Pudhom, T. Prueksaritanont, *RSC Adv.* **13** (2023) 29004 (https://doi.org/10.1039/D3RA04720B)
4. G. C. Fanning, F. Zoulim, J. Hou,A. Bertoletti, *Nat. Rev. Drug. Discov.* **18** (2019) 827 (https://doi.org/10.1038/s41573-019-0037-0)
5. X.Zhang, J.Cheng, J.Ma, Z. Hu, S. Wu, N. Hwang, J. Kulp, Y. Du, J.T. Guo, J. Chang, *ACS Infect. Dis.* **5** (2019) 759 (https://doi.org/10.1021/acsinfecdis.8b00269)
6. J. Sanchitra, A. Debnath, A.K. Singh, A.K. Jha, R. K. Singh, *Sci. Rep.* **15** (2025) 13054 (https://doi.org/10.1038/s41598-025-97242-6)
7. A. Mohebbi, S. P. T. Nabavi, M. Naderi, K. Sharifian, F. Behnezhad, M. Mohebbi, A. Gholami, F. S. Askari, A. Mirarab, S. H. Monavari, *In Silico Pharmacol.* **13** (2025) 35 (https://doi.org/10.1007/s40203-025-00314-8)
8. K. Vandyck, G. Rombouts, B. Stoops, A. Tahri, A. Vos, W. Verschueren, Y. Wu, J. Yang, F. Hou, B. Huang, K. Vergauwen, P. Dehertogh, J. M. Berke, P. Raboisson, *J. Med. Chem.* **61** (2018) 6247 (https://doi.org/10.1021/acs.jmedchem.8b00654)
9. S. Ejeh, A. Uzairu, G. A. Shallangwa, S. E. Abechi, *Future J. Pharm. Sci.* **7** (2021) 219 (https://doi.org/10.1186/s43094-021-00373-6)
10. S. Ejeh, A. Uzairu, G. A. Shallangwa, S. E. Abechi, M. T. Ibrahim, *Bull. Natl. Res. Cent.***46** (2022) 109 (https://doi.org/10.1186/s42269-022-00796-y)
11. A. Laoud, F. Ferkous, L. Maccari, G. Maccari, Y. Saihi,K. Kraim, *Comput. Biol. Chem.***72** (2018) 122 (https://doi.org/10.1016/j.compbiolchem.2017.12.003)
12. H. Nour, O. Daoui, O. Abchir, S. Elkhattabi,S. Belaidi, S. Chtita, *Heliyon* **8** (2022) e11991 (https://doi.org/10.1016/j.heliyon.2022.e11991)
13. O. Mafethe, T. Ntseane, T. H. Dongola, A. Shonhai, N. J. Gumede, F. Mokoena, *ACS Omega* **8** (2023) 38220 (https://doi.org/10.1021/acsomega.3c04494)
14. S. Mirzaei, R. Ghodsi, F. Hadizadeh, A. Sahebkar, *Biomed. Res. Int.* **6** (2022) 9761279 (https://doi.org/10.1155/2021/6480804)
15. N. Chahbaoui, S. Khamouli, M. Alaqarbeh, S. Belaidi, L. Sinha, S. Chtita, M. Bouachrine, *J. Biomol. Struct. Dyn.* **42** (2024) 12021 (https://doi.org/10.1080/07391102.2023.2266502)
16. D. A.Omoboyowa, *Chem. Africa* **5** (2022) 871 (https://doi.org/10.1007/s42250-022-00373-w)
17. C. Hanwarinroj, N. Phusi, B. Kamsri, P. Kamsri, A. Punkvang, S. Ketrat, P. Saparpakorn, S. Hannongbua, K. Suttisintong, P. Kittakoop, J. Spencer, A. J. Mulholland, P. Pungpo, *Future Med. Chem.* **14** (2022) 717 (https://doi.org/10.4155/fmc-2021-0348)
18. A. Belafriekh, A. Laoud, L. Mchichi, M. Bouachrine, *Phys. Chem. Res.* **12** (2024) 729 (https://doi.org/10.22036/pcr.2024.425052.2448)
19. F. Olawale, O. Iwaloye, K. Olofinsan, O. M. Ogunyemi, G. A. Gyebi, I. M. Ibrahim, *Chem. Pap.* **76** (2022) 3729 (https://doi.org/10.1007/s11696-022-02128-w)
20. A. K. Maurya,V. Mulpuru, N. Mishra, *ACS Omega* **5** (2020) 32234 (https://doi.org/10.1021/acsomega.0c03871)
21. A. Ali, M. H. Abdellattif, A. Ali, O. Abuali, M. Shahbaaz, M. J. Ahsan, M. A. Hussien, *Molecules* **26** (2021) 5932 (https://doi.org/10.3390/molecules26195932)
22. A. Laoud, F. Ali-Rachedi,F. Ferkous, *Phys. Chem. Res.* **11** (2023) 459 (https://doi.org/10.22036/pcr.2022.342259.2106)

23. A. A. Poola, P. S. Prabhu, T. P. K. Murthy, M. Murahari, S. Krishna,M. Samantaray, A. Ramaswamy, *Front. Mol. Biosci.* **10** (2023) 1106128 (https://doi.org/10.3389/fmolb.2023.1106128)
24. K. Tabti, S. Baammi, A. Sbai, H. Maghat, M. Bouachrine, *J. Biomol. Struct. Dyn.* **41** (2023) 13798 (https://doi.org/10.1080/07391102.2023.2183032)
25. M. A. Azam, J. Thathan, S. Jupudi, *Comput. Biol. Chem.* **84** (2020) 107197 (https://doi.org/10.1016/j.compbiolchem.2019.107197)
26. M. Elbouhi, K. Tabti, M. Ouabane, M. Alaqarbeh, K. Elkamel, T. Lakhlifi, A. Sbai, M. Bouachrine,*Chem. Heterocycl. Compd.* **60** (2024) 627 (https://doi.org/10.1007/s10593-025-03386-8)
27. S. Ahmad, D. Gupta, T. Ahmed, A. Islam, *J. Biomol. Struct. Dyn.* **41** (2023) 14016 (https://doi.org/10.1080/07391102.2023.2176361)
28. U. Panwar, S. K. Singh, *Struct. Chem.* **32** (2021) 337 (https://doi.org/10.1007/s11224-020-01628-3)
29. R. Dias, W. F. J. de Azevedo, *Curr. Drug Targets* **9** (2008) 1040 (https://doi.org/10.2174/138945008786949432)
30. V. M. Kulkarni, S. Bhansali, *Res. Reports Med. Chem.* **4** (2014) 1 (https://doi.org/10.2147/rrmc.s50738).